Published in final edited form as:

Structure. 2024 February 01; 32(2): 177–187.e5. doi:10.1016/j.str.2023.11.006.

The roles of FUS-RNA binding domain and low complexity domain in RNA-dependent phase separation

Laura R. Ganser[1], **Amirhossein Ghanbari Niaki**[1], **Xincheng Yuan**[1,2,3], **Ethan Huang**[1], **Dahlia Deng**[2,3], **Nathalie A. Djaja**[1,2,3], **Yingda Ge**[1], **Alanna Craig**[1], **Olivia Langlois**[1], **Sua Myong**[1,2,3,4,*]

[1]Department of Biophysics, Johns Hopkins University, Baltimore, MD 21218, USA

[2]Program in Cell, Molecular, Developmental Biology, and Biophysics, Johns Hopkins University, 3400 N Charles St, Baltimore, MD 21218, USA

[3]Department of Biology, Johns Hopkins University, 3400 N Charles St, Baltimore, MD 21218, USA

[4]Lead contact

SUMMARY

Fused in sarcoma (FUS) is an archetypal phase separating protein asymmetrically divided into a low complexity domain (LCD) and an RNA binding domain (RBD). Here, we explore how the two domains contribute to RNA-dependent phase separation, RNA recognition, and multivalent complex formation. We find that RBD drives RNA-dependent phase separation but forms large and irregularly shaped droplets that are rescued by LCD in *trans*. Electrophoretic mobility shift assay (EMSA) and single-molecule fluorescence assays reveal that, while both LCD and RBD bind RNA, RBD drives RNA engagement and multivalent complex formation. While RBD alone exhibits delayed RNA recognition and a less dynamic RNP complex compared to full-length FUS, LCD in *trans* rescues full-length FUS activity. Likewise, cell-based data show RBD forms nucleolar condensates while LCD in *trans* rescues the diffuse nucleoplasm localization of full-length FUS. Our results point to a regulatory role of LCD in tuning the RNP interaction and buffering phase separation.

Graphical Abstract

*Correspondence: smyong@jhu.edu.

AUTHOR CONTRIBUTIONS

L.R.G., A.G.N., and S.M designed experiments. L.R.G., X. Y., A.G.N., E.H., D.D., N.A.D, A.C., and O.L. conducted experiments. L.R.G and S.M. wrote the paper.

SUPPLEMENTAL INFORMATION

Supplemental information can be found online at https://doi.org/10.1016/j.str.2023.11.006.

DECLARATION OF INTERESTS

The authors declare no competing interests.

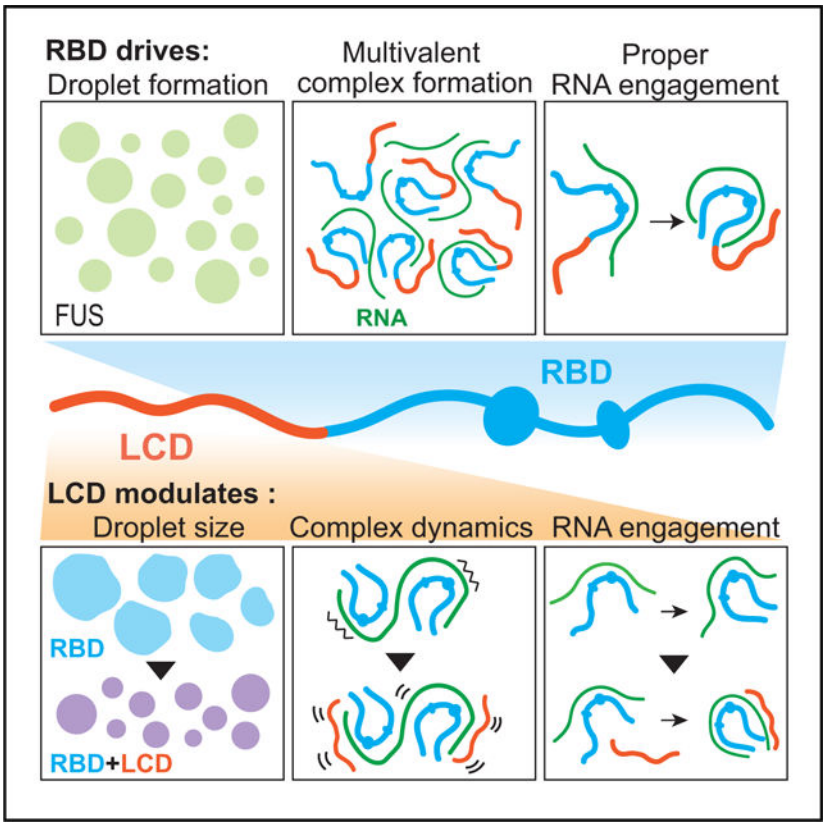

In biref

Ganser et al. investigate the molecular interactions underlying FUS phase separation in the presence of RNA, revealing distinct roles for the RBD and LCD. While RBD drives RNA recognition, multivalent complex formation, and phase separation, the LCD critically modulates the RNP interaction to maintain activity *in vitro* and in cells.

INTRODUCTION

Fused in sarcoma (FUS) is an abundant nuclear RNA binding protein (RBP) that helps to regulate nearly every level of RNA processing including splicing, transcription, polyadenylation, microRNA processing, and mRNA transport.[1,2] FUS undergoes liquid-liquid phase separation (LLPS) *in vitro*[3–5] and *in vivo*,[6–9] and this process may be important for the cellular activities of FUS. Additionally, aberrant LLPS of FUS contributes to pathogenic aggregation in neurodegenerative diseases, amyotrophic lateral sclerosis (ALS) and frontotemporal dementia (FTD). As is the case for many phase separating proteins,[10] FUS is asymmetrically organized into a prion-like low complexity domain (LCD) and an RNA binding domain (RBD).[11] FUS RBD is comprised of multiple RNA binding motifs including three disordered RGG-rich motifs, an RNA recognition motif (RRM), and a zinc finger domain (ZnF) (Figure 1A).

It has previously been reported that the FUS LCD is the primary driver of phase separation.[12–14] However, these studies relied on crowding agents and/or high

concentrations (>120 μM) to achieve phase separation with the LCD alone. Thus, LLPS of full-length FUS, which occurs around 5 μM in the absence of a crowding agent, is much more favorable than LCD alone.[11] Recently, interactions between the FUS LCD and RBD were found to be responsible for driving phase separation.[11,15,16] Specifically, cation-pi interactions between tyrosine residues in the LCD and arginine residues in the RBD were found to govern FUS phase separation.[11,16] An NMR study identified many heterogeneous interactions involving all residue types occurring between the FUS LCD and one of its RGG-rich motifs in the condensed state.[17] Thus, although arginine-tyrosine interactions are likely the dominant interactions driving LLPS, the full suite of interactions is likely more complicated and heterogeneous.

Another factor excluded in these studies is the effect of RNA on FUS LLPS. RNA is present for nearly all cellular activities of FUS, and over half of FUS is known to interact with RNA.[4] Therefore, it is critical to understand how the FUS-RNA interaction impacts FUS LLPS activity. RNA has been shown to buffer FUS phase separation by promoting condensation at low RNA:protein ratios and solubilizing FUS at high RNA:protein ratios.[3] Other studies have shown that RNA initiates LLPS for FUS and related proteins.[4,12,18,19] Here, we investigate the roles of the two FUS domains in the presence of RNA. First, we show that FUS RBD is the main driver of phase separation in the presence of equimolar RNA, while the LCD has roles in maintaining droplet size and morphology. Next, we apply biochemical and single-molecule fluorescence techniques to gain molecular-level insight on how the LCD modulates the FUS-RNA interaction. Together, our findings reveal the complementary roles built into RBD and LCD for RNA binding and RNA-dependent phase separation.

RESULTS

FUS RBD drives RNA-dependent phase separation

To investigate the roles of the two FUS domains (Figure 1A) on RNA-dependent condensation, we carried out phase separation assays using widefield microscopy for FUS RBD and LCD in the presence and absence of equimolar RNA using unstructured, single-stranded U40 RNA as done in previous studies.[5,20,21] We find that in the absence of RNA, neither LCD nor RBD form droplets up to 15 μM while full-length FUS forms droplets by at least 2.5 μM (Figures 1B and S1A). Adding LCD and RBD in *trans* (R + L) does not rescue droplet formation in the absence of RNA at concentrations up to 15 μM, indicating the importance of the physical link between RBD and LCD as in full-length FUS (Figures 1B and S1A). These results agree with previous results in the absence of RNA showing that LCD and RBD alone do not phase separate up to 30 μM while RBD+LCD in *trans* does not phase separate until ~25 μM compared to 5 μM for full-length FUS.[11] Given the +/− RNA results at the 1 μM condition, the addition of equimolar RNA may promote the phase separation of full-length FUS as has been seen previously (Figures 1B and S1A).[4] Strikingly, we find that RBD phase separates in the presence of RNA as readily as full-length FUS, whereas LCD does not form droplets in any conditions tested with RNA (Figures 1B and 1C). RBD and LCD in *trans* also undergo RNA-dependent phase separation similarly to full-length FUS and RBD alone. Dynamic light scattering (DLS), which is sensitive to very

small cluster (1–100 nm diameter) and droplet (1–10 μm) formation, further confirmed our results that FUS and RBD form micron-scale condensates (both ~100 nm clusters and ~1000 nm droplets were observed) while LCD remains dilute (10 nm diameter) in the presence of RNA (Figure S1B). Thus, while both the RBD and LCD in one molecule are required for efficient LLPS in the absence of RNA, we find that the RBD is necessary and sufficient to drive phase separation in the presence of RNA. Together these results support a role for RBD as the primary driver of RNA-dependent FUS phase separation.

FUS LCD maintains droplet size

From the phase separation assays, we observed that RBD droplets are substantially larger than full-length FUS droplets and qualitatively more irregular in shape (Figures 2A–2C). This result suggests a role for the LCD in maintaining droplet size and shape. In agreement with this prediction, adding LCD in *trans* (R + L) restores RBD droplet size to full-length FUS levels (Figure 2A). Although full-length FUS and RBD+LCD droplet sizes are significantly different based on the Student's t test, they have highly similar average sizes with overlapping error bars. This trend of large RBD droplets that were rescued by LCD in *trans* was observed at all concentrations and time points tested (Figures 2B and 2C). The increase in RBD droplet size compared to full-length FUS or R + L became more pronounced with increasing protein/RNA concentrations and with increasing droplet reaction times (Figures 2B and 2C). Furthermore, we found that increasing the concentration of LCD relative to RBD resulted in reduced droplet size in a dose-dependent manner with the effect plateauing around 3X the concentration of LCD to RBD (6 μM LCD and 2 μM RBD) (Figures 2D and 2E). To better understand how LCD is acting in *trans*, we carried out phase separation assays by doping in cy3-labeled RBD or cy3-labeled LCD with unlabeled LCD and RBD, respectively (Figure 2F). We found that RBD is roughly ~20- to 25-fold more concentrated than LCD in R + L droplets based on fluorescence intensity. Thus, a sub-stoichiometric concentration of LCD within the droplets is sufficient to reduce the droplet size. Add itionally, these data further support our finding that RBD-RNA interactions are the primary driver of phase separation rather than LCD-RBD and/or LCD-RNA interactions.

Interestingly, we did not observe any substantial change in the fluorescence recovery after photobleaching (FRAP) of RBD droplets with or without LCD present, despite the change in droplet size (Figure S2). Similar FRAP results were observed for RBD with and without LCD after bleaching the full droplet, bleaching partial droplets to observe only intra-droplet dynamics, and when the RBD was fluorescently labeled instead of the RNA molecule (Figure S2). The FRAP results were similar even under conditions where the difference in droplet size was more dramatic, including increasing the concentration of both RBD and LCD and increasing the relative amount of LCD to RBD (Figure S2). Thus, LCD appears to modulate droplet size without significantly changing the fluidic properties of the droplet at the concentrations and time points tested.

FUS LCD binds RNA but cannot form high-order complexes

We next sought to obtain a more molecular understanding of the activity of the two FUS domains. First, we demonstrate that both RBD and LCD truncations bind RNA using an Electrophoretic mobility shift assay (EMSA) gel (Figure 3). Although it was expected that

RBD would bind RNA, it was surprising that the LCD domain also bound RNA given that prion-like domains are not typically thought to have RNA-binding activity. We used an MBP-only negative control to ensure that this result was not due to non-specific binding to the MPB tag or protein contaminant (Figure S3). Like full-length FUS, both truncations form C1 and C2 complexes, which correspond to one and two units of FUS bound to the RNA strand, respectively (Figure 3).[5] Interestingly, C1 and C2 complexes run at the same height on the gel despite the proteins being substantially different sizes. This phenomenon was previously reported for FUS bound to various lengths of polyU RNA.[5] Although we do not fully understand why this occurs, it suggests that the overall FUS-RNA complex has a similar level of compaction regardless of FUS construct. Unlike full-length FUS and RBD, LCD does not form high-order complexes of protein and RNA, which agrees with the inability of LCD to form condensates (Figure 3). Interestingly, all constructs have similar affinity for RNA with the RNA-only band disappearing by 500 nM. Full-length FUS appears to have somewhat higher affinity based on the higher intensities of C1 and C2 at 10 nM and 50 nM, respectively (Figure 3). Together, the EMSA suggests that although both FUS domains can bind U50 RNA as monomers and dimers, the ability to form high-order complexes, presumably through multivalent interactions, is driven by the RBD and may be critical for droplet formation.

FUS LCD and RBD are both necessary for FUS:RNA dynamics

Next, we used single-molecule fluorescence resonance energy transfer (smFRET) to monitor the FUS-RNA interaction using a dual-labeled partial duplex RNA with a single-stranded polyuridine (U50) region for protein binding (Figure 4A). We first characterized the RNA-binding mode by monitoring the dynamics of the FUS-RNA interaction at equilibrium. Previous work found that monomer FUS binding (C1 in EMSA) resulted in a static high FRET signal while multimer binding (C2 in EMSA) yields a highly dynamic mid-FRET signal (Figure 4A).[5] In agreement with these previous results, we find that full-length FUS forms a highly dynamic complex with RNA at high concentration (500 nM) at which multimer binding is favored (Figure 4B). RBD, LCD, and R + L also yield a mix of static high-FRET and dynamic mid-FRET signal (Figure 4). Comparing the FRET values of the high-FRET signal and the mid-FRET fluctuations for all conditions suggests that the two states are the same across conditions (Figure S4). However, the dynamic state is substantially diminished for both RBD and LCD at 500 nM and instead, they are primarily in a static high-FRET conformation (Figures 4B and 4C). Strikingly, we find that adding RBD and LCD in *trans* (R + L) rescues FUS:RNA dynamics (Figure 4B). The loss in dynamics for RBD and LCD may indicate either that these truncations are less prone to form multimers on RNA or that multimer binding does not induce a dynamic interaction for the truncations as with full-length FUS (Figure 4A). Given the EMSA result showing that both truncations can indeed form the C2 multimer with similar affinities (Figure 3), we determine that it is primarily due to the loss of dynamics of the multimer conformation. These data show that both domains are critical for maintaining a dynamic FUS-RNA interaction. Since LCD is critical for complex dynamics at the molecular scale and for droplet size on the macroscale, it suggests a possible mechanism for LCD in maintaining droplet size by enhancing the dynamics of protein-RNA interactions. This is in line with previous results showing that dynamically arrested condensates are larger than more fluid condensates.[22]

FUS LCD promotes proper RNA engagement

We also used smFRET to monitor the initial moment of RNA binding that leads to C1 formation. Compared to the experiment shown in Figure 4, this experiment uses lower FUS concentration and is non-equilibrium to monitor monomer binding. As has been described previously, full-length FUS monomer (1–50 nM) binds via a well-ordered two-step process where initial contact results in a mid-FRET intermediate followed by a transition to a high-FRET state (Figure 5A).[5] The rate of both steps is dependent on the concentration of protein (Figures 5B and S5). RBD undergoes a similar two-step binding process, but the time between the first step (T1) and the second step (T2) is substantially longer, and a larger fraction of traces become trapped in the intermediate state without transitioning to the high-FRET state within the length of the movie (80 s) or before photobleaching (Figures 5B and S5). Furthermore, at 10 nM concentration, RBD binding shows FRET fluctuations in the intermediate state that suggest the protein is not as stably bound prior to reaching the high-FRET state (Figure 5B, left). The LCD also binds RNA, as was in the EMSA, but instead of undergoing a two-state process, it transitions directly to the high-FRET state (Figure 5C). This demonstrates that the RNA binding domain in RBD drives the two-state binding process and may suggest that this proper engagement of the RNA is critical for droplet formation. Strikingly, we see that LCD in *trans* rescues RBD activity by promoting and accelerating the second step (T2) to high-FRET (Figures 5C, 5D, and S5). The rate of the initial step (T1) is similar between full-length FUS, RBD, and R + L in agreement with the RBD mediating this step independently of the LCD (Figures 5D and S5). However, the time between steps (T2) is much longer for RBD alone than for R + L and especially for full-length FUS, demonstrating a role for LCD in promoting proper RNA engagement after the initial binding (Figures 5D and S5). Exactly how LCD promotes proper binding is unclear, but we carried out similar flow experiments with color-coded RBD and LCD and demonstrated that both RBD and LCD can bind the same RNA molecule (Figure S6). Thus, a physical interaction between the two domains and the RNA is a possible mechanism for the altered binding.

The RGG1 domain is necessary but not sufficient for droplet formation

RGG motifs are common RNA binding domains found in many RNA binding proteins that undergo phase separation.[23] RGG domains are unstructured and have little sequence specificity for RNA but are known to substantially increase the RNA binding affinity.[24–26] We sought to determine the role of the RGG domain in FUS phase separation and RNA binding. First, we found that adding RGG1 to the LCD domain (LCD-RGG1) was not sufficient to rescue droplet formation (Figures 6A and 6B). Furthermore, binding of LCD-RGG1 to RNA occurs similarly to LCD alone. Like LCD, LCD-RGG1 binds RNA and forms both C1 and C2 complexes but not high-order complexes in EMSAs (Figure 6C). Likewise, in smFRET experiments, LCD-RGG1 directly induces the high-FRET state without going through an intermediate as was observed for LCD (Figures 6D and 6E). At 50 nM, LCD-RGG binds RNA somewhat faster than LCD (~5 s versus ~16 s, respectively), which may suggest that LCD-RGG has a higher affinity for RNA although the difference is not observed at 10 nM or in the EMSA (Figures 5B, 5D, and 6C–6F). Regardless, the RGG domain does not rescue droplet formation, the high-order complex formation in EMSAs or

the intermediate state in smFRET binding assays. This suggests that the RGG1 domain is insufficient for driving droplet formation or proper RNA engagement.

On the other hand, removing the RGG1 domain from RBD (RBDDRGG1) prevents phase separation at 1 μM concentration with equimolar RNA (Figures 6A and 6B). Thus, the RGG1 domain is necessary but not sufficient for phase separation in these conditions. Interestingly, RBDDRGG forms C1 and high-order complexes but not C2 in the EMSA (Figure 6C). This suggests that the RGG domain is critical for FUS multi-merization on the RNA, although the mechanism for that is unclear. In smFRET experiments, binding of RBDDRGG1 to RNA goes through an intermediate state as with RBD alone or full-length FUS (Figure 6D), supporting the conclusion that the RGG1 domain does not drive proper RNA engagement. However, at 10 nM (C1 predominant concentration), the intermediate state is much less stable for RBDDRGG1 than for the full RBD based on the prevalence of fluctuations between mid-and low-FRET states (Figure 6D). Together, these data suggest that the RGG motif is not responsible for the intermediate state, but does help stabilize it, especially at low concentrations.

The RRM domain drives proper RNA engagement

We next tested the role of the RRM domain on droplet formation and RNA binding. RRM domains are common structured RNA binding domains that bind RNA with varying affinity and specificity.[19] The FUS RRM has low sequence specificity and has been reported to bind an NYNY quartet where N is any nucleotide and Y is any pyrimidine.[25] To test the role of the RRM, we used a FUS mutant with an RNA-binding deficient RRM, 4FL (F305L/F341L/F359L/F368L), and with four phenylalanine to leucine point mutations in the RRM (Figure 6A).[27] We found that FUS 4FL forms aberrant droplets that are substantially smaller than full-length FUS droplets, suggesting that FUS with a dysfunctional RRM cannot form proper condensates (Figure 6B). In the EMSA, 4FL still binds RNA and forms C1 and C2, but not higher-order complex, similar to LCD and LCD-RGG1 (Figures 6C and S5). This suggests that the RRM is responsible for the high-order complex formation, while other regions of FUS, such as the RGG motifs or zinc finger domain, are responsible for the C1 and C2 complex formation. FUS 4FL also binds RNA more similarly to LCD and LCD-RGG1 in the smFRET assays in that it primarily binds via a one-step transition to high FRET rather than through an intermediate. This supports a role for RRM as the driver of the intermediate state and proper RNA engagement. A percentage of traces (12% and 40% at 10 nM and 50 nM, respectively) do bind through an intermediate (Figure 6D). This may indicate an incomplete knockout of RNA-binding in the RRM with the mutant, which may also explain the formation of small droplets with 4FL. Regardless, the four point mutations in FUS 4FL have a dramatic effect on RNA binding and droplet formation, highlighting the importance of the FUS RRM on RNA recognition and multivalent complex formation.

LCD remains diffused in nucleoplasm while RBD phase separates into nucleoli

We expressed GFP-tagged full-length FUS, LCD, RBD, and 4FL in HeLa cells to examine the cellular localization and condensation behavior. Full-length FUS remains soluble in nucleoplasm as expected from the RNA buffering phase separation of FUS (Figures 7A and S7A).[3] LCD also exhibits a diffuse pattern, consistent with the *in vitro* pattern of no

condensation (Figures 7B and S7B). Interestingly, RBD-FUS, which drives phase separation into large condensates *in vitro*, co-condenses into the nucleolus which is highly enriched with RNA (Figures 7C and S7C). It is likely that the RNA binding affinity of RBD drives it to localize to the nucleoli where it condenses in the presence of RNA. Importantly, this reveals a new role of LCD in preventing FUS from localizing into nucleoli. The RNA-binding deficient mutant, 4FL-FUS, which forms aberrant aggregation *in vitro* forms bright puncta throughout the nucleoplasm representing aggregate formation (Figures 7D and S7D). Since RNA buffers phase separation of FUS, 4FL-FUS with deficient RNA binding, likely condenses and aggregates.

In vitro, we demonstrated that LCD interacts with RBD in *trans*. While RBD alone exhibits delayed RNA engagement, less dynamic RNP complex and larger condensate formation compared to full-length FUS, adding the LCD in *trans* rescues the full-length FUS activity, suggesting a role for LCD in optimizing the RBD-RNA interaction required for proper RNA contact and condensate formation. We tested if expressing RBD and LCD in *trans* would rescue the full-length FUS pattern in cells. Indeed, when LCD was co-transfected with RBD in *trans*, the nucleolar RBD localization was strikingly reduced, recovering the diffuse pattern exhibited by the full-length FUS protein (Figure 7E, second row, Figures S7E–S7G). Although it is impossible to know the exact amount of protein expressed based on the amount of transfected DNA, we observed that this rescue effect was LCD dose dependent as the recovery was more complete with higher concentrations of LCD-expressing plasmid transfected (Figure 7E, third row), mirroring what was seen *in vitro* (Figure 2D). Taken together, the cellular results support an RBD-LCD interaction and are aligned with the central findings of our *in vitro* study.

DISCUSSION

Our results demonstrate the importance of the RBD and RNA in FUS phase separation. Although the LCD is often considered the main driver of phase separation, we find that the RBD is in fact sufficient for phase separation in the presence of RNA and at low concentrations (1–15 μM). In these conditions, LCD was neither necessary nor sufficient for phase separation. Although most studies exclude RNA, the RNA-binding domain of hnRNPA1 was previously shown to also undergo LLPS in the presence of RNA independent of its LCD, suggesting this may be a general phenomenon.[18] Furthermore, it is well established that RNA promotes phase separation for most, if not all, phase separating proteins. Although this is partially due to non-specific interactions such as complex coacervation, our results provide evidence that specific RBP-RNA interactions are critical to LLPS. Thus, studies that rely only on the LCD to approximate LLPS activity or exclude RNA may miss critical molecular forces driving LLPS. Our study used unstructured polyU RNA for simplicity, but future studies will examine more physiologically relevant RNAs such as SON-GGU mRNA[25] and G-quadruplex RNA[28] to explore the importance of RNA sequence and structure.

Previously, interactions between FUS RBD and LCD were found to drive LLPS in the absence of RNA.[11,15,16] Specifically, cation-pi interactions between tyrosine residues in the LCD and arginine residues in the RBD were found to be the major contributors to FUS

phase separation.[11,16] This explained why neither RBD nor LCD alone underwent LLPS below 30 μM but did phase separate at ~25 μM when added in *trans*. Our results reproduced these results in the absence of RNA and additionally found that RBD phase separates in the presence of RNA at a much lower concentration,~1 μM. This demonstrates that the interactions between RBD and RNA are a more significant driver of phase separation than the interactions between RBD and LCD. There are many reasons why RBD-RNA interactions may be stronger than RBD-LCD interactions. Arginine residues in the RBD can also form cation-pi stacking interactions with RNA bases similarly to the tyrosine residues in LCD. In this study, the RNA has 40 bases capable of these interactions compared to the 27 tyrosine residues in the LCD. There is also the additional electrostatic interaction between the positively charged arginine residues and the RNA backbone. In comparison, the LCD only has four negative charges. Finally, the RNA recognition by the RRM and ZnF provides additional interactions compared to RBD-LCD interactions. Thus, the same principle of multivalent interactions as described for FUS in the absence of RNA applies in the presence of RNA, but the RBD-RNA interactions become the dominant driving force.

In support of a combinatorial effect of multiple RBD-RNA interactions, we found that both the RRM and RGG1 are critical for FUS phase separation. Removing RGG1 increased the C_{sat} and prevented droplets at the tested conditions, likely by decreasing the number of RNA-protein interactions. We identified a role for the RRM in proper RNA engagement which appears to be critical for high-order complex formation in EMSAs and droplet formation in LLPS assays. Additional FUS truncations and mutations can be used to obtain a more detailed view of each FUS region.

Although the LCD does not drive LLPS in the presence of RNA, we did identify an important role for the LCD in modulating the FUS-RNA interaction which appears to have implications on the droplet size. Single molecule experiments revealed that without the LCD, RBD alone formed a less-dynamic interaction with RNA compared to full-length FUS which was rescued by adding LCD in *trans*. Likewise, adding LCD in *trans* rescued proper RNA engagement. This role for the LCD is in-line with the model put forth by Franzmann and Alberti that LCDs have chaperone-like behavior rather than being autonomous aggregation modules.[29] Although the exact mechanism remains to be determined, our results suggest that the LCD interacts with the RBD or RNA (or likely both) and helps to promote proper RBD-RNA interactions possibly by keeping the interaction dynamic and preventing trapped conformations. Future studies could investigate whether our results are specific to the FUS LCD or if other LCDs would have the same effect on droplet size and RNA interactions. Our results suggest that this modulation at the molecular level manifests in the size and shape of droplets, highlighting the connection between molecular level interactions and droplet properties.

The cellular localization and diffuse pattern for LCD is consistent with our *in vitro* observation that LCD remains soluble in solution. Unexpectedly, RBD localizes to and co-condenses with nucleoli. This is reminiscent of the condensate induced by transcription inhibition where FUS and other RNA binding proteins such as SFPQ, NONO, and TAF15 translocate to nucleoli upon inhibition of RNAP II.[30,31] Our observation that RBD localizes to nucleoli even in the absence of transcription inhibition indicates that RBD is necessary

and sufficient to localize to nucleoli and such translocation is prevented by the LCD. In this regard, the LCD is a negative regulator of RBD, and such regulation is lifted when transcription is inhibited to allow for FUS localization to nucleoli. The nucleolar localization of RNA binding proteins can be driven by specific nucleolar transcripts,[32] but more in-depth study is required to elucidate the mechanistic basis and biological significance of RBD localization to nucleoli.

Intriguingly, the addition of LCD in *trans* rescued the aberrant behavior of RBD both *in vitro* and in cells. The physical interaction between the two highly asymmetric domains even in crowded cellular environment is remarkable and shows the level of tight coupling between the LCD and RBD that constitute FUS. The dose-dependent effect of LCD in overcoming the RBD induced nucleolar localization again reveals the role of LCD in suppressing RBD mislocalization to nucleoli. These findings point out an interesting possibility that FUS exhibits different LCD-RBD conformational states as required by different cellular needs. Future studies will be directed toward investigating the roles of both domains in cellular pathways (Figure 8).

Although the functional implications of our results remain to be determined, there is evidence that the physical properties and underlying molecular interactions of condensates give rise to their functional behaviors and that misregulation of these properties is linked to pathology.[33] For example, larger and less circular (irregular) granules are displayed in pathologic conditions such as cells generated from IPSC of neurodegenerative patients or when mutant FUS protein is expressed in mammalian cells.[34] In such conditions, splicing of FUS target mRNA is compromised.[35] Thus, understanding the interplay of different interactions underpinning droplet properties can help reveal the mechanism of FUS-RNA phase separation and will likely have implications on the regulation of FUS activity in both healthy and disease states.

STAR★METHODS

RESOURCE AVAILABILITY

Lead contact—Further information and requests for resources and reagents should be directed to and will be fulfilled by the Lead Contact, Sua Myong (smyong@jhu.edu).

Materials availability—All unique reagents generated in this study are available from the lead contact without restriction.

Data and code availability

- Matlab (https://www.mathworks.com/), IDL (http://www.exelisvis.co.uk/Products Services/IDL.aspx), FIJI (https://imagej.nih.gov/ij/), OriginLab (https://www.originlab.com/), and NIS-Elements Ar Package (https://www.microscope.healthcare.nikon.com) software is available online from the respective distributers. Single Molecule FRET data acquisition and analysis package can all be obtained freely from the website (https://cplc.illinois.edu/software/).

- In-house Matlab code was published previously[20] and is publicly available online at Zenodo (https://doi.org/10.5281/zenodo.5866686).
- Any additional information required to reanalyze the data reported in this paper is available from the lead contact upon request.

EXPERIMENTAL MODEL AND STUDY PARTICIPANT DETAILS

***E. coli* culturing—**All expression plasmids were transformed into competent BL21 (DE3) E. *coli* cells (NEB) and grown in LB media with 50 μg/mL Kanamycin. Cells were added 1:1 to 50% (v/v) glycerol and stored at −80°C.

Mammalian cell culture—HeLa cells (ATCC) were grown at 37°C with 5% CO_2 in a DMEM solution supplemented with 10% FBS, 2 mM glutamine, 100 mg/mL Pen-Strep, 0.1 mM non-essential amino acids, and 1 mM sodium pyruvate. A T75 flask with 10 mL DMEM was used to grow and passage cells. Cells were washed with 1X distilled PBS before trypsinizing with 0.05% trypsin. The trypsinized cells were neutralized by 10X addition of DMEM. Cells were diluted to 1:10 in new flasks. Cells were grown on 4-well glass bottom chambers for 24 hours prior to transfection. Transfection was performed through calcium phosphate precipitation, using 2.5 M $CaCl_2$ and 2X HEPES buffered saline pH 7.0 (274 mM NaCl, 10 mM KCl, 1.4 mM $Na_2HPO_4{\cdot}7H_2O$, 15 mM dextrose, 42 mM HEPES). For long-term storage, cells were trypsinized, DMSO was added to a final concentration of 5% (v/v) cells, and cells were frozen at −80°C before being transferred to liquid nitrogen.

METHOD DETAILS

Protein preparation—Proteins preparation was done as described previously.[5] Bacterial expression plasmids for all FUS constructs were fused to a 6xHis-MBP tag at the N terminus with a TEV cleavage site between this tag and the FUS sequence. Plasmids were purchased (Genscript) with codon-optimization for E. *coli* expression. The expression plasmids were transformed into BL21 (DE3) competent E. *coli* cells (NEB). Cells were grown in LB media with 50 μg/mL Kanamycin at 37°C in until an OD_{600} of ~0.4. At this point, protein expression was induced with 0.25 mM IPTG for 2 hr at 30°C. Cells were harvested and lysed by sonication in lysis buffer (1 M KCl, 1 M Urea, 50 mM Tris-HCl, pH 7.4, 10 mM imidazole, 1.5 mM b-mercaptoethanol, 1% NP-40, 5% glycerol, protease inhibitor tablet, and RNase). Lysed cells were centrifuged at 23,000 xg at 4°C for 30 min and the supernatant was passed through a 0.2 μM filter. Cell Lysis was then passed through a HisTrap FF Crude column (cytiva), using an AKTA pure 25M FPLC system (GE) using FUS binding buffer (1 M KCl, 1 M Urea, 50 mM Tris-HCl, pH 7.4, 1.5 mM b-mercaptoethanol, 5% glycerol, 10 mM imidazole). Proteins were eluted with imidazole by applying a linear gradient of elution buffer (1M KCl, 1 M Urea, 50 mM Tris-HCl, pH 7.4, 1.5 mM b-mercaptoethanol, 5% glycerol, 500 mM imidazole). FUS-containing fractions showing the correct size were stored in 30% Glycerol at 4°C or flash frozen and stored at −80°C for long term storage.

When required, proteins were labeled at free amine groups (lysine side chains and N-terminal amine) using Cy3-NHS ester dye. First the protein was exchanged into reaction buffer (100 mM sodium phosphate, 150 mM NaCl, pH 7.5) using a zeba column

(ThermoFisher). For the reaction,~10 μM protein was mixed with ~4X dye and incubated 20 min in the dark. Free dye was removed with two additional runs through fresh zeba columns. For experiments with fluorescently labeled LCD protein, a lysine residue was added to the C-terminus of the LCD sequence for labeling since there is no natural lysine in the sequence. There was no difference in activity with this construct.

RNA preparation—RNA was purchased (IDT) containing appropriate modifications. For droplet reactions, 3′ amine modifications were added for labeling with Cy3 NHS esters. For smFRET, the strand containing the sequence of interest was modified at the 5′ end with an amine for Cy3 labeling and the 18-nucleotide sequence was added at the 3′ end to form the partial duplex. The complementary 18-mer sequence was purchased with an amine modification on the 3′ end for Cy5 labeling and a biotin modification at the 5′ end for tethering to the single molecule surface.

To label the RNA, a 50 μL reaction mixture of 20 μM amine-modified RNA and 0.1 mg Cy3- or Cy5- NHS ester in 100 mM sodium bicarbonate was incubated overnight in the dark at room temperature. The labeled RNA was purified via two rounds of ethanol precipitation. After incubation, 3 μL 5 M NaCl and 125 μL 100% ice cold ethanol were added to the reaction followed by a 30 min incubation at −20°C and a 30 min centrifugation at 21000 xg and 4°C. The resulting pellet was rinsed with 70% ethanol and resuspended in 50 μL T50 buffer (10 mM Tris-HCl pH 8.0, 50 mM NaCl). The process was then repeated, and the final pellet was fully dried before being resuspended in T50 buffer for use.

RNA stocks were stored in water or T50 buffer at −20°C. Before use, the single stranded RNAs for droplet reactions were subjected to heat denaturation (85°C for 2–3 min) and rapid cooling on ice for ~20 min. The partial duplex RNA for smFRET experiments were annealed by mixing 10 μM of the biotinylated Cy5 strand and 12–15 μM of the Cy3 strand in T50 buffer and heating to 85°C for 3 minutes with slow cooling to 5°C at the rate of 2°C/min.

Widefield microscopy phase separation assays—Purified protein containing a 6xHis-MBP-tag was buffer exchanged into 20 mM sodium phosphate pH 7.4 using a centrifugal filter (Amicon, Millipore). Droplet reactions were set up by mixing protein and RNA at the desired concentrations in cleavage buffer (100 mM Tris-HCl, pH 7.5, 100 mM NaCl, 1 mM EDTA, 1 mM DTT). Unless otherwise noted, 10 nM Cy3-labeled RNA was added to the reaction for visualization. In some cases, 10 nM Cy3-labeled protein was added instead. TEV protease (~0.1 μL/ 3 mg protein) was added to cleave the 6xHis-MBP tag and initiate the droplet reaction. Droplets formed on the surface of Nunc Lab-Tek 8-well chambers or Cellvis glass bottom 96-well chambers and were imaged in the brightfield and/or Cy3 channel using a Nikon Ti Eclipse widefield microscope with 100x oil immersive objective spanning an area of ~133 × 133 μm^2.

For FRAP experiments, a 50 mW bleaching laser at 405 nm and a Brucker galvano mirror scanner were used to bleach full or partial droplets. Fluorescence recovery was measured immediately after bleaching by acquiring images in the cy3 channel for 12 min at a rate of

1 image every 3 sec for the first 2 min and 1 image every 10 sec for the remaining 10 min. Data was processed with an in-house matlab script as described previously.[5]

Dynamic light scattering—Reaction mixtures were prepared as in the widefield microscopy phase separation assays and transferred to a non-binding 96-well plate for imaging. All reaction components were filtered using a 0.22 μm syringe filter. Equimolar (1 μM) protein and RNA concentrations were used in all experiment. DLS results were acquired with Wyatt DynaPro Plate Reader II (Wyatt Technology) and transformed into size distribution by the Dynamic 7 software (Wyatt Technology). After extracting the distributions into a set of .csv files, a MATLAB script was applied to visualize the data.

EMSA—Binding reactions were set up with increasing protein concentration (0–500 nM) and 1 nM Cy3/Cy5-labeled partial duplex U50 RNA (same as smFRET construct) in EMSA binding buffer (50 mM Tris-HCl, pH 7.5, 150 mM KCl, 2 mM MgCl2, 100 mM b-mercaptoethanol, 0.1mg/mL BSA). The reactions were incubated ~15 min in the dark at room temperature and then ran on a 6% DNA retardation polyacrylamide gel (Invitrogen) using 0.5X TBE running buffer at 150 V. Gels were imaged using a Typhoon scanner (GE Healthcare) in both Cy3 and Cy5 channels.

Single molecule FRET—Single molecule slides were prepared as previously described.[5,36] Quartz slides and glass coverslips were treated with sequential sonication in detergent, methanol, acetone, and 1 M KOH with water washes after each step. The slides and coverslips were then burned with flame until dry. They were then incubated in a solution of 1% (v/v) aminosilane and 5% acetic acid (v/v) in methanol for 20 min in the dark. This solution was washed off and the slides/coverslips dried with nitrogen gas before being treated with a mixture of 98% mPEG (m-PEG-5000, Laysan Bio, Inc.) and2% biotin PEG (biotin-PEG-5000, Laysan Bio, Inc). After an incubation overnight, the PEG passivated slides were thoroughly washed with water, dried with nitrogen gas, and stored at −20°C.

The dual-labeled partially duplexed smFRET U50 RNA was tethered to the single molecule surface with a biotin-neutravidin linkage by treating with 0.2 mg/mL neutravidin in T50 buffer, washing with T50 buffer, and adding ~25 pM RNA in T50 buffer. The slides were washed with T50 buffer again and then treated with imaging buffer (20 mM Tris-HCl, pH 7.5, 100 mM KCl, 0.5 w/v % glucose, 1 mg/mL glucose oxidase, 1.8 U/mL catalase, 5–10 mM Trolox). Protein was diluted in imaging buffer and added to the slides to measure the protein-RNA interactions. A syringe pump was used to pull 50 μL protein onto the surface at a rate of 1 mL/min with a 10 sec delay. Images and movies were recorded using a home-built prism-type TIRF-FRET microscope. Each imaged region contained about 300–600 molecules.

Cell based experiments—HeLa cells (ATCC) were grown at 37°C with 5% CO_2 in a DMEM solution supplemented with 10% FBS, 2 mM glutamine, 100 mg/mL Pen-Strep, 0.1 mM non-essential amino acids, and 1 mM sodium pyruvate. Cells were washed with 1X distilled PBS before trypsinizing with 0.05% trypsin. The trypsinized cells were neutralized by 10X addition of DMEM. Cells were diluted to 1:10 in new flasks.

Cells were grown on 4-well glass bottom chambers for 24 hours prior to transfection. Transfection was performed through calcium phosphate precipitation, using 2.5 M $CaCl_2$ and 2X HEPES buffered saline pH 7.0 (274 mM NaCl, 10 mM KCl, 1.4 mM $Na_2HPO_4{\cdot}7H_2O$, 15 mM dextrose, 42 mM HEPES). Cells were transfected with 0.1 ug of GFP tagged FUS constructs (LCD, RBD and 4FL), unless otherwise specified. Cells were fixed 24 hours after transfection in formaldehyde diluted to 4% in 1X PBS for 10 min at room temperature. Cells were permeabilized and blocked in buffer (0.3% Triton™ X-100 and 1% BSA in 1X PBS) for 10 min. Hoechst dye was diluted in buffer and incubated with the cells for 1 hour at room temperature. Cells were washed with 1X PBS and maintained in 1X PBS at 4°C after staining and imaged the same day via confocal microscopy.

Confocal microscopy was performed with a Zeiss LSM 700 microscope equipped with lasers for 405, 488, 568, and 647 nm excitation. Images were acquired using four-fold frame averaging with a 63 × 1.4 oil objective. The same laser and acquisition settings were maintained for imaging all samples within one experiment.

QUANTIFICATION AND STATISTICAL ANALYSIS

Processing and quantification of droplet images—Droplet images were acquired and saved using the Nis-Element AR software (Nikon). For each condition, at least five images of representative fields of view (~133 × 133 μm^2) were taken. Fiji software was used to convert images to TIFF and adjust the brightness and contrast as necessary to best visualize the droplets. Images were transferred to Illustrator (Adobe) to crop and compile finalized figures. Droplet size was quantified using in-house Matlab scripts (analyzeDroplets.m and batch_analyzeDroplets.m, https://zenodo.org/record/5866686). FRAP images were analyzed using an in-house Matlab script described previously[5] (FRAP_analyzer_AGHN.m, https://zenodo.org/record/5866686) that includes corrections for background, photobleaching, and droplet drift. Graphs of droplet size and FRAP were plotted in OriginLab and the relevant statistical information is listed in the associated figure legends. Figures were finalized in Illustrator (Adobe).

EMSA quantification—Gel images taken in the Cy5 channel were quantified using FIJI's gel analysis function. The intensity of each band was determined as the area under the curve of the intensity plot with background correction. The intensity of each band was normalized to the total intensity of the corresponding lane after background correction. Graphs of the normalized intensity was plotted in OriginLab and the relevant statistical information is listed in the associated figure legends. Figures were finalized in Illustrator (Adobe).

Single-molecule data analysis—Single molecule videos were processed using IDL as described previously.[37] Processed data was visualized with MatLab using in-house scripts (Trace_Viewer_Categorizer_AHGN.m, https://zenodo.org/record/5866686). For flow images, the first (T1) and second (T2) binding steps were recorded for each trace. T1 (adjusted for delay before flow) and DT (T2-T1) values for all traces from three replicates were plotted and fit to an exponential decay (ExpoDecay1: $y=y_0+A1*\exp(-(x-x_0)/t1)$) in OriginLab to determine the rate and standard error. Violin plots were generated in

Matlab (Violin_plot.m, https://zenodo.org/record/5866686). Figures generated in Matlab or OriginLab were finalized in Illustrator (Adobe).

Supplementary Material

Refer to Web version on PubMed Central for supplementary material.

ACKNOWLEDGMENTS

We thank the members of Sua Myong and Taekjip Ha laboratory for helpful discussion and insights. We also thank the Integrated Imaging Center at Johns Hopkins for providing the Typhoon for EMSA gels. This work was supported by NIH grants F32GM139268 (to L.R.G.), 1 1 RF1NS113636-01 (to S.M.), and F31NS124267 (to N.A.D).

INCLUSION AND DIVERSITY

While citing references scientifically relevant for this work, we also actively worked to promote gender balance in our reference list.

REFERENCES

1. Ratti A, and Buratti E (2016). Physiological functions and pathobiology of TDP-43 and FUS/TLS proteins. J. Neurochem 138, 95–111. [PubMed: 27015757]
2. Lagier-tourenne C, Polymenidou M, and Cleveland DW (2010). TDP-43 and FUS/TLS: emerging roles in RNA processing and neurodegeneration. Hum. Mol. Genet 19, 46–64.
3. Maharana S, Wang J, Papadopoulos DK, Richter D, Pozniakovsky A, Poser I, Bickle M, Rizk S, Guillén-Boixet J, Franzmann TM, et al. (2018). RNA buffers the phase separation behavior of prion-like RNA binding proteins. Science 360, 918–921. [PubMed: 29650702]
4. Schwartz JC, Wang X, Podell ER, and Cech TR (2013). RNA Seeds Higher-Order Assembly of FUS Protein. Cell Rep. 5, 918–925. [PubMed: 24268778]
5. Niaki AG, Sarkar J, Cai X, Rhine K, Vidaurre V, Guy B, Hurst M, Lee JC, Koh HR, Guo L, et al. (2020). Loss of Dynamic RNA Interaction and Aberrant Phase Separation Induced by Two Distinct Types of ALS/FTD-Linked FUS Mutations. Mol. Cell 77, 82–94.e4. [PubMed: 31630970]
6. Saitoh N, Spahr CS, Patterson SD, Bubulya P, Neuwald AF, and Spector DL (2004). Proteomic Analysis of Interchromatin Granule Clusters. Mol. Biol. Cell 15, 3876–3890. [PubMed: 15169873]
7. Sama RRK, Ward CL, Kaushansky LJ, Lemay N, Ishigaki S, Urano F, and Bosco DA (2013). FUS/TLS assembles into stress granules and is a prosurvival factor during hyperosmolar stress. J. Cell. Physiol 228, 2222–2231. [PubMed: 23625794]
8. Kanai Y, Dohmae N, and Hirokawa N (2004). Kinesin Transports RNA: Isolation and Characterization of an RNA-Transporting Granule. Neuron 43, 513–525. [PubMed: 15312650]
9. Yang L, Gal J, Chen J, and Zhu H (2014). Self-assembled FUS binds active chromatin and regulates gene transcription. Proc. Natl. Acad. Sci. USA 111, 17809–17814. [PubMed: 25453086]
10. Wiedner HJ, and Giudice J (2021). It's not just a phase: function and characteristics of RNA-binding proteins in phase separation. Nat. Struct. Mol. Biol 28, 465–473. [PubMed: 34099940]
11. Wang J, Choi JM, Holehouse AS, Lee HO, Zhang X, Jahnel M, Maharana S, Lemaitre R, Pozniakovsky A, Drechsel D, et al. (2018). A Molecular Grammar Governing the Driving Forces for Phase Separation of Prion-like RNA Binding Proteins. Cell 174, 688–699.e16. [PubMed: 29961577]
12. Burke KA, Janke AM, Rhine CL, and Fawzi NL (2015). Residue-by-Residue View of In Vitro FUS Granules that Bind the C-Terminal Domain of RNA Polymerase II. Mol. Cell 60, 231–241. [PubMed: 26455390]

13. Patel A, Lee HO, Jawerth L, Maharana S, Jahnel M, Hein MY, Stoynov S, Mahamid J, Saha S, Franzmann TM, et al. (2015). A Liquid-to-Solid Phase Transition of the ALS Protein FUS Accelerated by Disease Mutation. Cell 162, 1066–1077. [PubMed: 26317470]

14. Kato M, Han TW, Xie S, Shi K, Du X, Wu LC, Mirzaei H, Goldsmith EJ, Longgood J, Pei J, et al. (2012). Cell-free formation of RNA granules: Low complexity sequence domains form dynamic fibers within hydrogels. Cell 149, 753–767. [PubMed: 22579281]

15. Bogaert E, Boeynaems S, Kato M, Guo L, Caulfield TR, Steyaert J, Scheveneels W, Wilmans N, Haeck W, Hersmus N, et al. (2018). Molecular Dissection of FUS Points at Synergistic Effect of Low-Complexity Domains in Toxicity. Cell Rep. 24, 529–537.e4. [PubMed: 30021151]

16. Qamar S, Wang G, Randle SJ, Ruggeri FS, Varela JA, Lin JQ, Phillips EC, Miyashita A, Williams D, Ströhl F, et al. (2018). FUS Phase Separation Is Modulated by a Molecular Chaperone and Methylation of Arginine Cation-p Interactions. Cell 173, 720–734.e15. [PubMed: 29677515]

17. Murthy AC, Tang WS, Jovic N, Janke AM, Seo DH, Perdikari TM, Mittal J, and Fawzi NL (2021). Molecular interactions contributing to FUS SYGQ LC-RGG phase separation and co-partitioning with RNA polymerase II heptads. Nat. Struct. Mol. Biol 28, 923–935. [PubMed: 34759379]

18. Molliex A, Temirov J, Lee J, Coughlin M, Kanagaraj AP, Kim HJ, Mittag T, and Taylor JP (2015). Phase Separation by Low Complexity Domains Promotes Stress Granule Assembly and Drives Pathological Fibrillization. Cell 163, 123–133. [PubMed: 26406374]

19. Ganser LR, Djaja NA, and Myong S (2023). Biochemical and structural biology aspects of liquid–liquid phase separation: an interplay between proteins and RNA. In Droplets of Life, Uversky VN, ed. (Academic Press), pp. 133–155.

20. Rhine K, Dasovich M, Yoniles J, Badiee M, Skanchy S, Ganser LR, Ge Y, Fare CM, Shorter J, Leung AKL, and Myong S (2022). Poly(ADP-ribose) drives condensation of FUS via a transient interaction. Mol. Cell 82, 969–985.e11. [PubMed: 35182479]

21. Rhine K, Makurath MA, Liu J, Skanchy S, Lopez C, Catalan KF, Ma Y, Fare CM, Shorter J, Ha T, et al. (2020). ALS/FTLD-Linked Mutations in FUS Glycine Residues Cause Accelerated Gelation and Reduced Interactions with Wild-Type FUS. Mol. Cell 80, 666–681.e8. [PubMed: 33159856]

22. Linsenmeier M, Hondele M, Grigolato F, Secchi E, Weis K, and Arosio P (2022). Dynamic arrest and aging of biomolecular condensates are modulated by low-complexity domains, RNA and biochemical activity. Nat. Commun 13, 3030. [PubMed: 35641495]

23. Thandapani P, O'Connor TR, Bailey TL, and Richard S (2013). Defining the RGG/RG Motif. Mol. Cell 50, 613–623. [PubMed: 23746349]

24. Bonucci A, Murrali MG, Banci L, and Pierattelli R (2020). A combined NMR and EPR investigation on the effect of the disordered RGG regions in the structure and the activity of the RRM domain of FUS. Sci. Rep 10, 20956. [PubMed: 33262375]

25. Loughlin FE, Lukavsky PJ, Kazeeva T, Reber S, Hock EM, Colombo M, Von Schroetter C, Pauli P, Cléry A, Mühlemann O, et al. (2019). The Solution Structure of FUS Bound to RNA Reveals a Bipartite Mode of RNA Recognition with Both Sequence and Shape Specificity. Mol. Cell 73, 490–504.e6. [PubMed: 30581145]

26. Ozdilek BA, Thompson VF, Ahmed NS, White CI, Batey RT, and Schwartz JC (2017). Intrinsically disordered RGG/RG domains mediate degenerate specificity in RNA binding. Nucleic Acids Res. 45, 7984–7996. [PubMed: 28575444]

27. Daigle JG, Lanson NA Jr., Smith RB, Casci I, Maltare A, Monaghan J, Nichols CD, Kryndushkin D, Shewmaker F, and Pandey UB (2013). RNA-binding ability of FUS regulates neurodegeneration, cytoplasmic mislocalization and incorporation into stress granules associated with FUS carrying ALS-linked mutations. Hum. Mol. Genet 22, 1193–1205. [PubMed: 23257289]

28. Takahama K, Takada A, Tada S, Shimizu M, Sayama K, Kurokawa R, and Oyoshi T (2013). Regulation of telomere length by G-quadruplex telomere DNA- and TERRA-binding protein TLS/FUS. Chem. Biol 20, 341–350. [PubMed: 23521792]

29. Franzmann TM, and Alberti S (2019). Prion-like low-complexity sequences: Key regulators of protein solubility and phase behavior. J. Biol. Chem 294, 7128–7136. [PubMed: 29921587]

30. Yasuhara T, Xing YH, Bauer NC, Lee L, Dong R, Yadav T, Soberman RJ, Rivera MN, and Zou L (2022). Condensates induced by transcription inhibition localize active chromatin to nucleoli. Mol. Cell 82, 2738–2753.e6. [PubMed: 35662392]

31. Yang L, Zhang J, Kamelgarn M, Niu C, Gal J, Gong W, and Zhu H (2015). Subcellular localization and RNAs determine FUS architecture in different cellular compartments. Hum. Mol. Genet 24, 5174–5183. [PubMed: 26123490]

32. Wang M, Tao X, Jacob MD, Bennett CA, Ho JJD, Gonzalgo ML, Audas TE, and Lee S (2018). Stress-Induced Low Complexity RNA Activates Physiological Amyloidogenesis. Cell Rep. 24, 1713–1721.e4. [PubMed: 30110628]

33. Mathieu C, Pappu RV, and Taylor JP (2020). Beyond Aggregation: Pathological Phase Transitions in Neurodegenerative Disease. Science 370, 56–60. [PubMed: 33004511]

34. Djaja NA, Chang MT, Beinart FR, Morris VM, Ganser LR, and Myong S (2023). Nucleation and Dissolution Mechanism Underlying Amyotrophic Lateral Sclerosis/Frontotemporal Lobar Dementia-Linked Fused in Sarcoma Condensates. iScience 26, 106537. [PubMed: 37123224]

35. Sun S, Ling S-C, Qiu J, Albuquerque CP, Zhou Y, Tokunaga S, Li H, Qiu H, Bui A, Yeo GW, et al. (2015). ALS-Causative Mutations in FUS/TLS Confer Gain and Loss of Function by Altered Association with SMN and U1-SnRNP. Nat. Commun 6, 6171. [PubMed: 25625564]

36. Ganser LR, Ge Y, and Myong S (2023). Single-Molecule Fluorescence Methods to Study Protein-RNA Interactions Underlying Biomolecular Condensates. Methods Mol. Biol 2563, 149–160. [PubMed: 36227472]

37. Roy R, Hohng S, and Ha T (2008). A practical guide to single-molecule FRET. Nat. Methods 5, 507–516. [PubMed: 18511918]

Highlights

- In the presence of RNA, FUS RBD is necessary and sufficient for phase separation
- FUS RBD drives proper RNA engagement and multivalent complex formation via the RRM
- LCD does not drive phase separation but modulates droplet size and shape
- The LCD promotes proper FUS-RNA engagement and dynamics at the molecular level

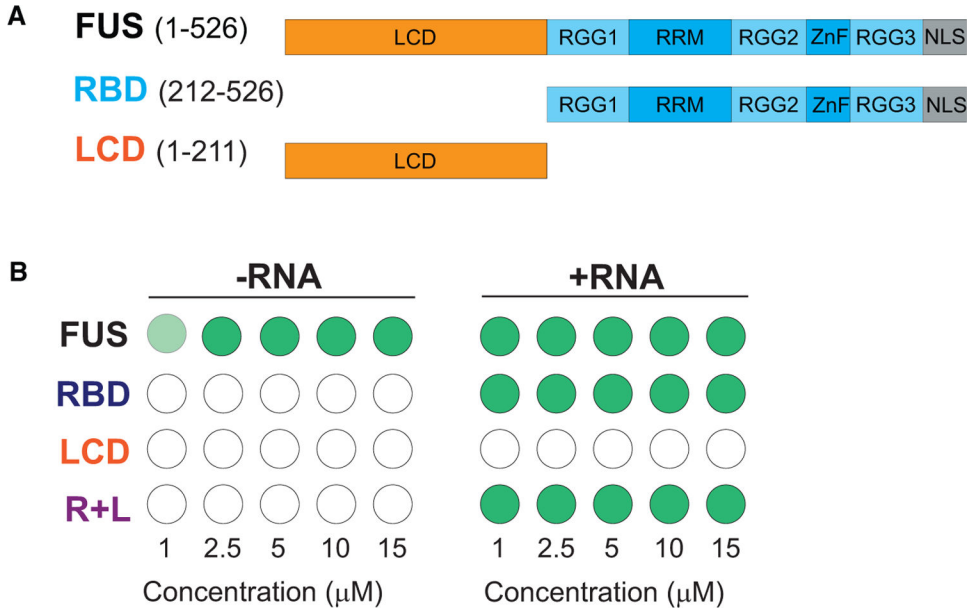

Figure 1. FUS RBD drives RNA-dependent phase separation

(A) Schematic of FUS constructs. (LCD, low complexity domain; RBD, RNA binding domain; RGG, RGG motif; RRM, RNA recognition motif; ZnF, zinc finger domain; NLS, nuclear localization signal) (B) Summary of phase separation assay results for protein with or without equimolar U40-cy3 RNA. At least three replicates were taken for each condition. Green indicates droplet formation, faded green indicates inconsistent droplet formation, and white indicates no droplet formation. See also Figure S1.

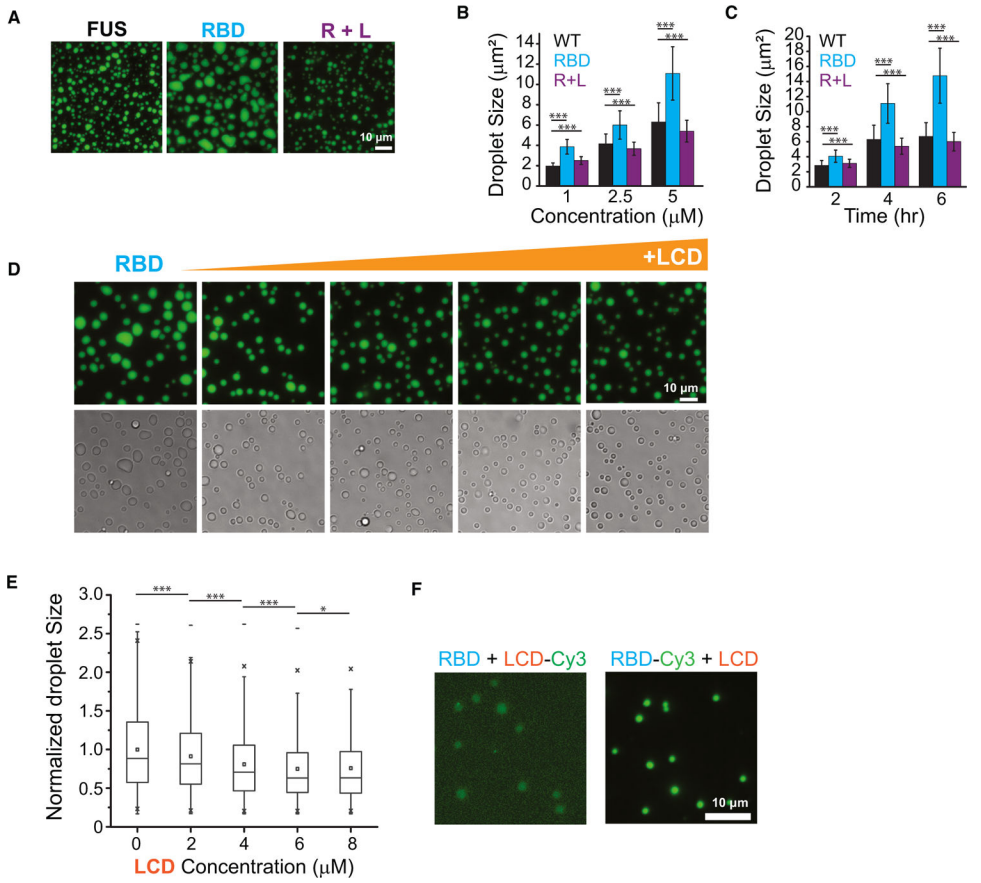

Figure 2. LCD maintains droplet size

(A) Representative fluorescence microscopy images of phase separation assay for protein at 5 μM with equimolar U40-Cy3 RNA. Image taken at 4 h time point. Scale bar is 10 μm.

(B) Quantified droplet size at increasing concentration taken at the 4 h time point. Statistics calculated using Student's t test where ***$p < 0.001$.

(C) Quantified droplet size at increasing droplet reaction time taken at the 5 μM concentration. All conditions have equimolar protein and U40-Cy3 RNA. The average and standard deviation from three replicates is shown. Statistics calculated using Student's t test where ***$p < 0.001$.

(D) Representative fluorescence microscopy and corresponding brightfield images for increasing LCD concentration (0,2,4,6, and 8 μM) added to 2 μM RBD. Image taken at 4 h time point. Scale bar is 10 μm.

(E) Data shown from three replicates with droplet size normalized to the average droplet size of the RBD alone condition. Mean (box), median (line), box edges: 25th and 75th percentile, whiskers: 5th and 95th percentile, X's: 1% and 99%, dash maximum value. Statistics calculated using Student's t test where *$p < 0.05$, ***$p < 0.001$.

(F) Representative fluorescence microscopy images of droplets formed with 1 μM each RBD, LCD, and U40 RNA taken at 4 h time point. Either LCD-Cy3 or RBD-Cy3 is added to visualize protein localization. Scale bar is 10 μm. See also Figure S2.

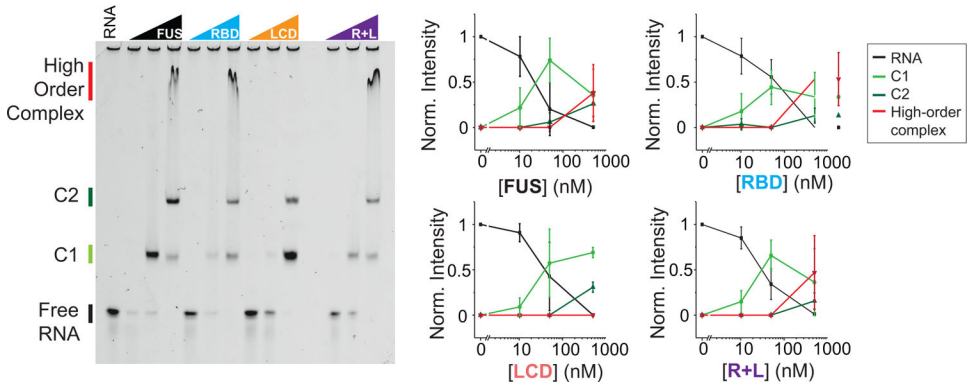

Figure 3. EMSA shows RNA binding activity for all FUS constructs, but LCD cannot form high-order complexes

(*left*) Representative EMSA gel with 1 nM labeled U50 RNA and increasing protein concentration from 10 to 500 nM. (*right*) Quantified band intensity normalized for each lane. The average and standard deviation from three replicates is shown. See also Figure S3.

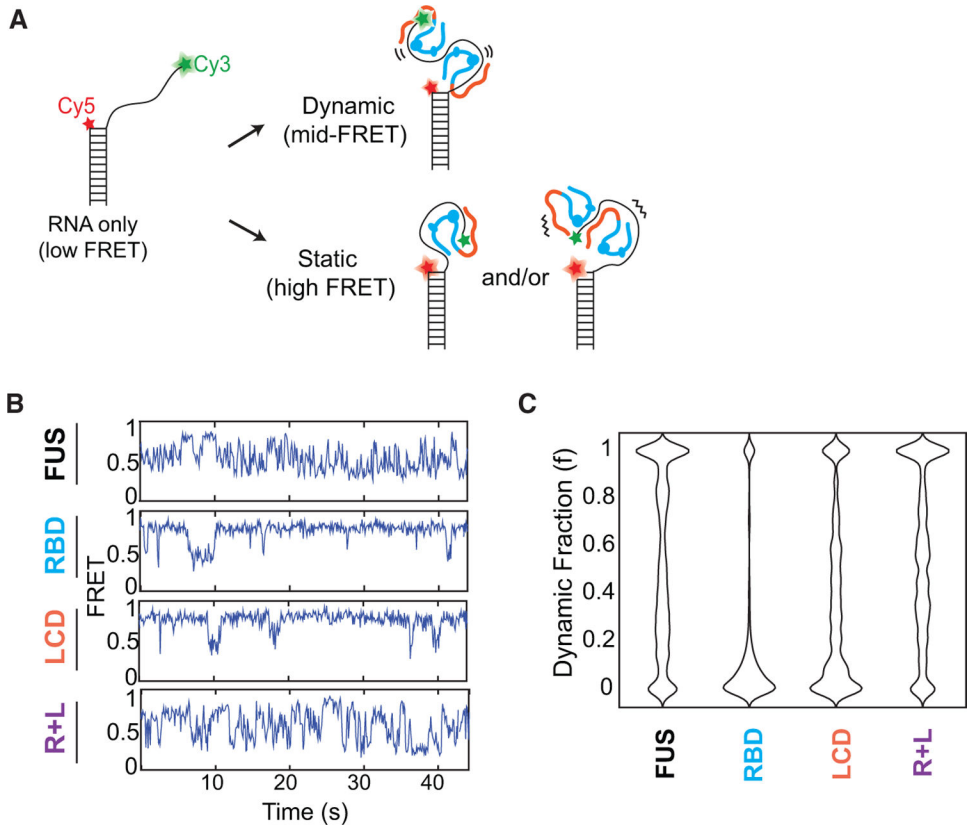

Figure 4. Both RBD and LCD are required for RNA:FUS dynamics at equilibrium

(A) Schematic of the smFRET binding assay. From previous work, single FUS binding induces a static high-FRET state and multimer FUS binding induces a dynamic mid-FRET state.

(B) smFRET results for each protein at 500 nM concentration after ~15 min incubation. (left) Representative traces.

(C) Violin plot showing the population density of the fraction of each trace in the mid-FRET dynamic trace averaged over >450 traces from three replicates. See also Figure S4.

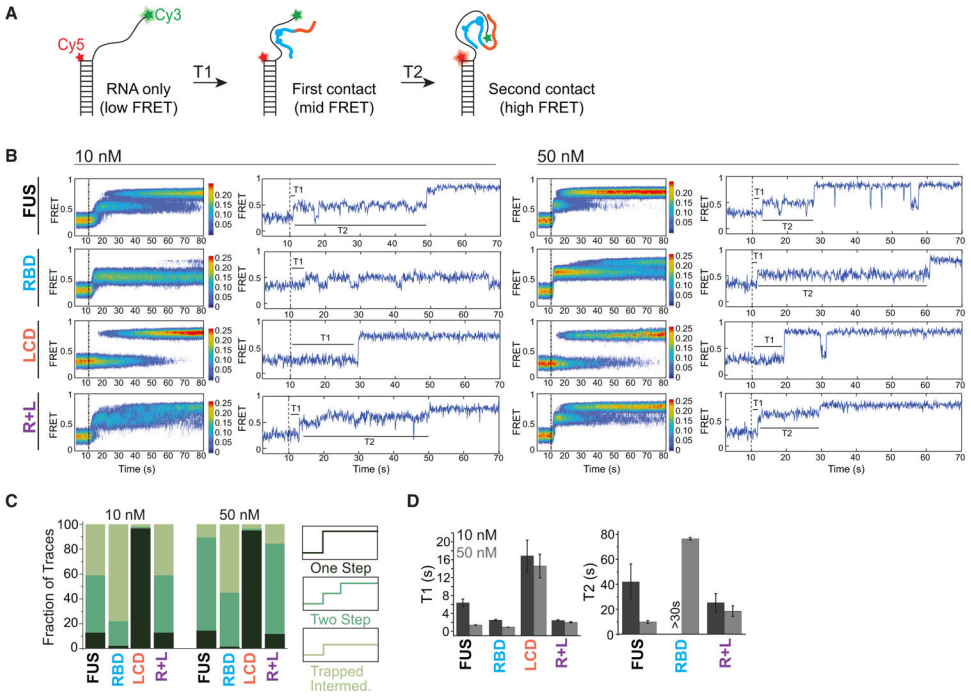

Figure 5. FUS LCD promotes proper RNA engagement

(A) FUS binding RNA occurs through a two-step mechanism involving a mid-FRET intermediate prior to the high-FRET monomer-bound state. T1 is the time between flowing protein and the first step while T2 is the time between the first and second step.

(B) smFRET flow experiments for 10 nM and 50 nM protein. Protein added after 10 s delay (dotted line). (*left*) Heatmaps of all traces from three replicates, 90–350 traces. (*right*) Representative traces (C). Fraction of flow traces categorized as one-step, two-step, or trapped intermediate for each protein condition.

(D) Time values for the first step (T1) for all trace categories and time between the first and second step (DT) for all two-step traces. Values from three replicates were fit to an exponential decay to determine the rate and standard error shown in plots (Figure S5). See also Figure S6.

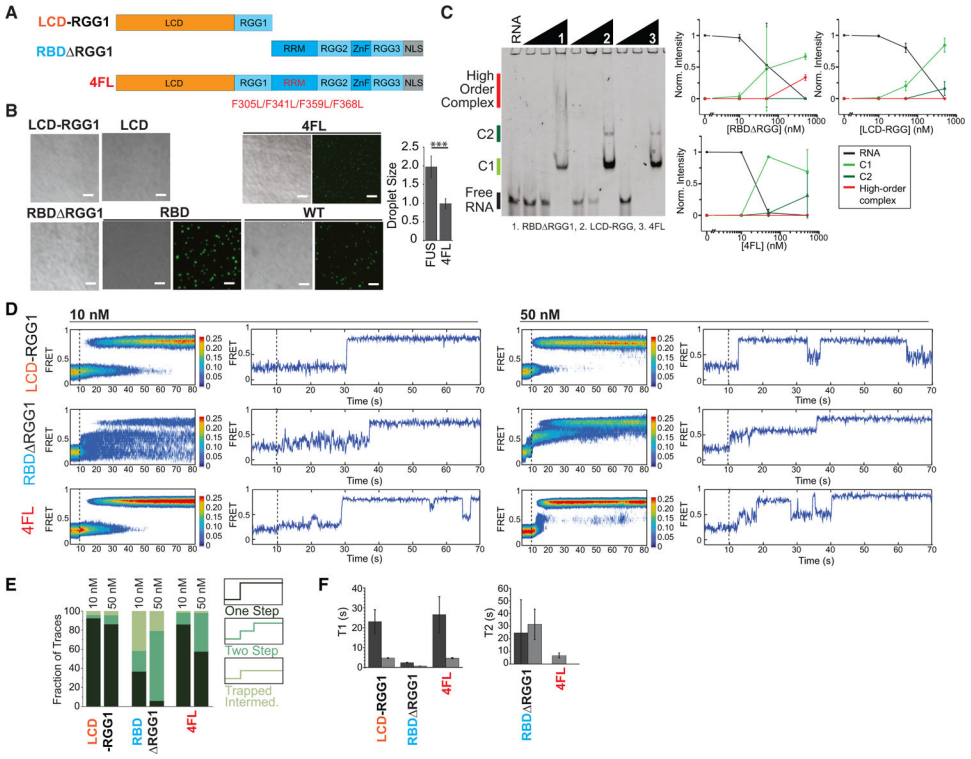

Figure 6. Additional FUS mutants reveal that RGG is necessary but not sufficient to drive RNA-dependent phase separation of FUS

(A) Schematic of FUS constructs. (LCD, low complexity domain; RBD, RNA binding domain; RGG, RGG motif; RRM, RNA recognition motif; ZnF, zinc finger domain; NLS, nuclear localization signal) (B). Representative fluorescence microscopy or DIC images of phase separation assay for protein at 1 μM with equimolar U40-Cy3 RNA. Image taken at 4 h time point. Scale bar is 10 μm. Comparison of droplet size for 4FL and full-length FUS. Average and standard deviation over three replicates are plotted. Statistics calculated using Student's t test where ***$p < 0.001$.

(C) EMSA analysis for three FUS variants. (*left*) Representative EMSA gel with 1 nM labeled U50 RNA and increasing protein concentration from 10 to 500 nM. (*right*) Quantified band intensity normalized for each lane. The average and standard deviation from three replicates is shown.

(D) smFRET flow experiments for 10 nM and 50 nM protein. Protein added after 10 s delay (dotted line). Representative traces (right) and heatmaps of all traces (left) from three replicates, 180–400 traces total.

(E) Fraction of flow traces categorized as one-step, two-step, or trapped intermediate for each protein condition.

(F) Time values for the first step (T1) for all trace categories and time between the first and second step (DT) for all two-step traces. Values from three replicates were fit to an exponential decay to determine the rate and standard error shown in plots (Figure S5).

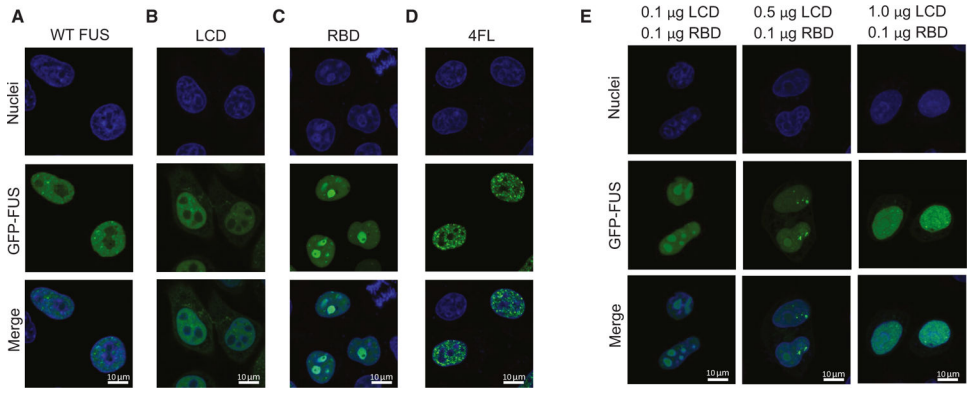

Figure 7. LCD remains diffuse in nucleoplasm while RBD phase separates into nucleoli

(A–D) N-terminally GFP tagged full-length FUS (A), LCD (B), RBD (C), and 4FL (D) are expressed in HeLa cells. Fluorescence images reveal diffuse pattern for full-length FUS (A) and LCD (B) in nucleoplasm. In contrast, RBD (C) entirely phase separates into nucleoli and 4FL mutant forms aggregate pattern throughout the nucleoplasm.

(E) LCD was titrated at 0.1 µg, 0.5 µg, and 1 µg to a fixed 0.1 µg of RBD. The nucleolar localization of RBD dissipates as a function of increasing LCD concentration, signifying LCD-RBD interaction in *trans* which results in recovery of full-length diffuse pattern and nucleoplasmic localization. See also Figure S7.

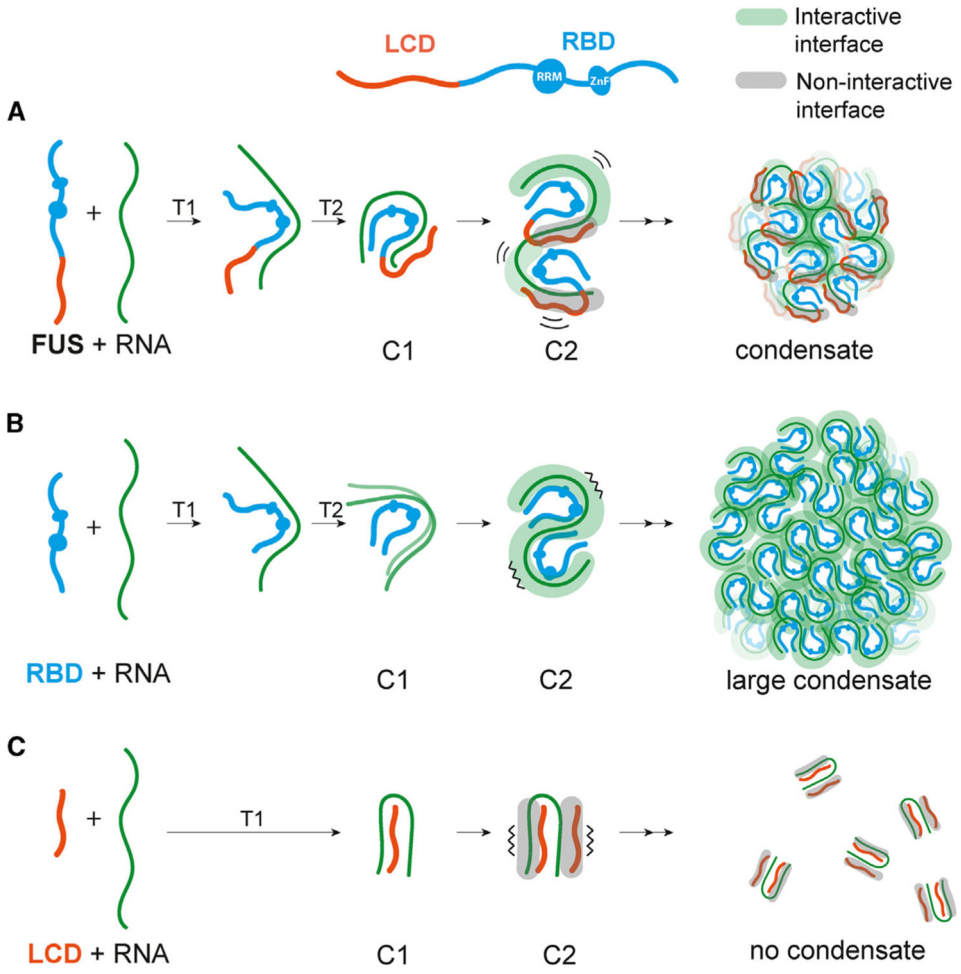

Figure 8. Schematic summary

(A) FUS-RNA interaction involves two-step binding process for C1 formation and dynamic FUS-RNA interaction of C2 state, which leads to proper condensate formation.

(B) RBD-RNA interaction displays a less stable C1 state and mostly static C2 state that results in large condensate, likely due to a higher degree of interactive interface produced by RBD-RNA contact.

(C) LCD-RNA interaction exhibits a sharp one-step binding to C1 and highly static C2 formation which is not conducive for condensate formation likely due to a non-interactive interface generated by the RNA-LCD interaction.

KEY RESOURCES TABLE

REAGENT or RESOURCE	SOURCE	IDENTIFIER
Bacterial and virus strains		
E. coli BL21(DE3) Chemically Competent Cells	Sigma-Aldrich	CMC0014
NEB Turbo Competent *E. coli* (High Efficiency)	New England Biolabs	C2984H
Chemicals, peptides, and recombinant proteins		
acTEV Protease	Fisher Scientific	12-575-015
Ribonuclease A from bovine pancreas	Millipore Sigma	R6513
RNase Inhibitor, Murine	New England Biolabs	M0314L
BSA	New England Biolabs	B9000S
Glucose Oxidase from Aspergilus niger	Sigma-Aldrich	G2133
Catalase from bovine liver	Sigma-Aldrich	C3155
cOmplete Mini EDTA-free Protease Inhibitor Cocktail	Roche	11836170001
Cy3 NHS Ester	Cytiva	PA13101
Cy5 NHS Ester	Cytiva	PA15100
IPTG	Gold Biotechnology	12481
Kanamycin monosulfate	Gold Biotechnology	K-120
Imidazole	Sigma-Aldrich	I5513
Aminosilane (N-(2-Aminoethyl)-3-Aminopropyltrimethoxysilane)	UCT Specialties	1760-24-3
m-PEG-SVA	Laysan Bio, Inc.	MPEG-SVA-5000-1g
Biotin-PEG-SVA	Laysan Bio, Inc.	Biotin-PEG-SVA-5000-1g
Neutravidin Protein	Thermo Scientific	31000
TROLOX	Thermo Scientific	218940050
DMEM, High Glucose, No glutamine	Thermo Scientific	11960-044
Fetal Bovine Serum, Certified, United States	Thermo Scientific	16000-044
Sodium Pyruvate (100mM)	Thermo Scientific	113-60-070
L-Glutamine (200mM)	Thermo Scientific	250-30-081
Penicillin-Streptomycin (10,000U/mL	Thermo Scientific	151-40-122
MEM Non-Essential Amino Acids Solution (100x)	Thermo Scientific	111-40-050
Trypsin-EDTA (0.05%), Phenol Red	Thermo Scientific	25300062
Hoechst 33342 Solution (20mM)	Thermo Scientific	62249
Formaldehyde Solution	Millipore Sigma	47608-1L-F
Experimental models: Cell lines		
Human: HeLa	ATCC	Cat# CCL-2; RRID: CVCL_0030
Oligonucleotides		
Biotin-18-mer: 5′- /biotin/rUrGrG rCrGrA rCrGrG rCrArG rCrGrA rGrGrC/3AmMO/ -3′	IDT	N/A
U50-18-mer: 5′-/5AmMC6/rUrUrU rUrUrU rUrUrU rUrUrU rUrUrU rUrUrU rUrUrU rUrUrU rUrUrU rUrUrU rUrUrU rUrUrU rUrUrU rUrUrU rUrUrU rUrUrU rUrUrG rCrCrU rCrGrC rUrGrC rCrGrU rCrGrC rCrA -3′	IDT	N/A

REAGENT or RESOURCE	SOURCE	IDENTIFIER
U40: 5′- rUrUrU rUrUrU rUrUrU rUrUrU rUrUrU rUrUrU rUrUrU rUrUrU rUrUrU rUrUrU rUrUrU rUrUrU rU/3AmMO/-3′	IDT	N/A
Recombinant DNA		
pTHMT/FUS_{WT} [encoding 6xHis-MBP-FUS WT (1-526)]	Niaki et al., 2020[5]	N/A
pTHMT/FUS_{LCD} [encoding 6xHis-MBP-FUS LCD (1-211)]	GenScript, this paper	N/A
pTHMT/FUS_{LCD-K} [encoding 6xHis-MBP-FUS LCD-K (1-211+Lys)]	GenScript, this paper	N/A
pTHMT/$FUS_{RBD}\Delta_{RGG}$ [encoding 6xHis-MBP-FUS RBDDRGG (268-526)]	GenScript, this paper	N/A
pTHMT/$FUS_{LCD-RGG}$ [encoding 6xHis-MBP-FUS LCD-RGG (1-267)]	GenScript, this paper	N/A
pTHMT/FUS_{4FL} [encoding 6xHis-MBP-FUS 4FL (F305L/F341L/F359L/F368L)]	GenScript, this paper	N/A
pFUS-WT-GFP_pcDNA3.1(+)-N-eGFP	Djaja, et al. 2023[34]	N/A
pFUS-LCD-GFP_pcDNA3.1(+)-N-eGFP	GenScript, this paper	N/A
pFUS-RBD-GFP_pcDNA3.1(+)-N-eGFP	GenScript, this paper	N/A
pFUS-4FL-GFP_pcDNA3.1(+)-N-eGFP	GenScript, this paper	N/A
Software and algorithms		
Matlab	Mathworks	https://www.mathworks.com/products/matlab.html
NIS-Elements Ar Package	Nikon Inc.	https://www.microscope.healthcare.nikon.com/
OriginLab 8.5	OriginLab	https://www.originlab.com/
ImageJ (Fiji)	NIH	https://imagej.nih.gov/ij/
smCamera	Roy et al.[37]	https://cplc.illinois.edu/research/tools
Interactive Data Language (IDL)	Harris Geospatial	https://www.l3harrisgeospatial.com/Software-Technology/IDL
Dynamic 7 software	Wyatt Technology	https://www.wyatt.com/products/software/dynamics.html
Illustrator	Adobe	https://www.adobe.com/products/illustrator.html
Zen Blue	Zeiss	N/A
Other		
HisTrap Fast Flow Crude	Cytiva	17528601
6% Polyacrylamide DNA Retardation Gel	Invitrogen	EC63655BOX
Amicon Ultra-0.5 Centrifugal Filter Unit (50K MWCO)	Millipore Sigma	UFC5050
Zeba Spin Desalting Columns, 7K MWCO, 0.5 mL	Thermo Scientific	89883
Nunc Lab-Tek Chambered Coverglass	Thermo Scientific	155411
96-well Glass Bottom Plate with High Performance #1.5 Cover Glass	Cellvis	P96-1.5H-N
non-binding 96-well plate	Corning	3881
E.Z.N.A. Plasmid DNA Mini Kit I, (V-spin)	Omega Bio-Tek	D6943-01
Nunc Lab-Tek Chambered Cover Glass, 4-wells	Thermo Scientific	155383PK